J. Fluid Mech. (1997), *vol.* 3443, *pp.* 303–316. Printed in the United Kingdom

The vaporization of a liquid front moving through a hot porous rock. Part 2. Slow injection

By ANDREW W. WOODS[1] AND SHAUN D. FITZGERALD[2]

[1]School of Mathematics, University of Bristol, Bristol BS8 1TW, UK

[2]Geothermal Program, Department of Petroleum Engineering, Stanford University, Stanford, CA 94305, USA

(Received 9 July 1996 and in revised form 7 March 1997)

We present a series of similarity solutions to describe the temperature field as liquid spreads from a line source into a porous rock saturated with liquid of higher temperature. We identify slow and fast flow regimes. In the slow flow regime, the liquid is heated to the far-field temperature by conduction of heat from the far field. In the fast flow regime, there is negligible conduction of heat from the far field. Instead, the liquid is heated to the far-field temperature by cooling a region of the host rock near the source, and an internal boundary layer develops within the newly injected liquid. We successfully test our quantitative theoretical predictions with a series of laboratory experiments in which water was injected into a consolidated bed of sand filled with liquid of different temperature. We extend our model to describe the vaporization of liquid as it spreads slowly from a central source into a superheated porous rock. A further family of similarity solutions shows that the rate of vaporization depends upon the injection rate as well as upon the initial superheat of the reservoir. For high injection rates, the liquid is typically heated to the interface temperature long before reaching the interface. The rate of vaporization then becomes independent of the initial liquid temperature, and depends mainly on the reservoir superheat. For lower injection rates, heat is conducted from ahead of the boiling front into the liquid. As a result, for progressively smaller injection rates, an increasing fraction of the liquid vaporizes, until virtually all the liquid boils, and only a very small liquid zone develops in the rock. Again, we successfully test our theoretical predictions with a laboratory experiment in which liquid water was injected into a superheated layer of permeable sandstone.

1. Introduction

There is a growing interest in the use of geothermal resources for the production of energy. Superheated geothermal systems provide one of the most attractive resources for such power generation since the thermal energy stored in the ground may be efficiently harnessed as high-enthalpy vapour (Grant, Donaldson & Bixley 1982; Elder 1981). However, as fluids are drawn from a reservoir, natural recharge may be unable to maintain the fluid reserves, and the associated pressure falls. This leads to a decline in the production potential of the reservoir. To compensate for this effect, various schemes for liquid reinjection have been developed (Barker, Koenig & Stark 1995; Enedy *et al.* 1993; Grant *et al.* 1982). As liquid migrates into a reservoir, part of the liquid vaporizes thereby restoring the pressure. In order to evaluate the

effectiveness of a recharge scheme, it is important to understand the fundamental controls on the mass fraction of the liquid which vaporizes and the temperature distribution in the liquid.

Pruess *et al.* (1987) and Woods & Fitzgerald (1993; hereafter called Part 1), analysed the rapid injection, migration and vaporization of liquid into geothermal reservoirs. Under such circumstances, the dynamic pressure associated with the newly formed vapour controls the saturation temperature at the boiling interface and hence the mass fraction of liquid which vaporizes (see the Appendix). In addition, for such rapid liquid migration, thermal diffusion has a negligible role in the heat transfer. Therefore, the rock ahead of the vaporizing liquid front does not cool until it is invaded by the front. Furthermore, owing to the thermal inertia of a permeable rock, isotherms advance more slowly than the liquid itself, and so liquid is heated up to the interfacial temperature long before reaching the interface. This rapid injection regime is therefore inefficient in that the thermal energy used to heat up the large body of water behind the interface to the vaporization temperature is not immediately available for vaporization of the liquid.

In the present continuation of the work, we describe the very different flow regime which develops if the liquid is injected into the reservoir so slowly that the effects of heat conduction become important. For such slow injection, the vapour pressure remains nearly uniform and close to the original reservoir pressure (Appendix; Fitzgerald & Woods 1995). Now, conduction of heat from the far field controls the vaporization process, affecting both the temperature distribution in the liquid and the mass fraction of liquid which vaporizes. The slow injection regime may develop as liquid migrates into the hot rock from a vertical well-bore.

We present a new class of similarity solutions which identify how the temperature field evolves as fluid of one temperature displaces fluid of a second temperature within a permeable porous layer. We successfully compare our model with a series of carefully controlled laboratory experiments, and we then extend the model to account for vaporization when the liquid slowly invades a superheated permeable rock. Finally we discuss the application of our results to developing strategies of liquid-injection in geothermal systems.

2. Thermal evolution of liquid–liquid displacements

We describe the two-dimensional axisymmetric spreading of a volume flux of liquid, $2\pi Q$ per unit length, from a central source through a porous rock of porosity ϕ and permeability k (figure 1). We assume the temperature of the liquid on injection is T_o and that the host rock is initially saturated with liquid of temperature T_2. In §4, we extend the analysis to include the effects of vaporization.

The Darcy velocity at radius r in the liquid is purely radial and has the value

$$u = Q/r. \tag{2.1}$$

The temperature T evolves with time t according to the thermal advection–diffusion equation

$$\frac{\partial T}{\partial t} + \frac{\lambda_w Q}{r}\frac{\partial T}{\partial r} = \frac{\kappa}{r}\frac{\partial}{\partial r}\left(r\frac{\partial T}{\partial r}\right) \tag{2.2}$$

where κ is the average thermal diffusivity (Batchelor 1974) and the constant λ_w represents the dimensionless heat capacity of the liquid, made dimensionless by the

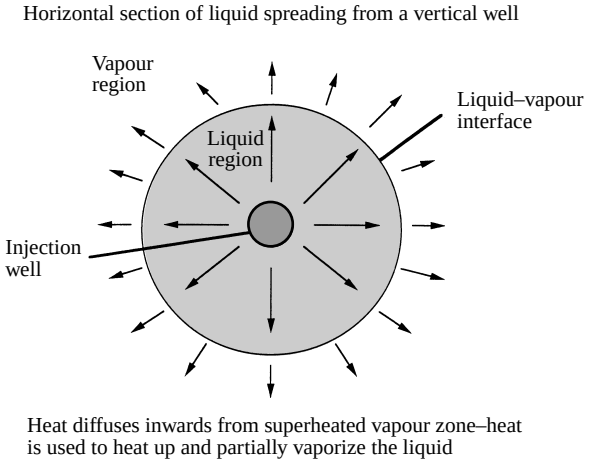

FIGURE 1. Schematic of the injection geometry. Arrows on the figure represent the direction of the flow.

mass-averaged heat capacity of the liquid ($\rho_l C_{pl}$) and solid matrix ($\rho_s C_{ps}$),

$$\lambda_w = \rho_l C_{p_l}/[\rho_l C_{p_l}\phi + \rho_s C_{p_s}(1-\phi)]. \tag{2.3}$$

λ_w is typically of order unity: for example for liquid water invading sandstone of porosity 0.35, $\rho_l C_{pl} = 4.05 \times 10^6\,\mathrm{J\,m^{-3}\,K^{-1}}, \rho_s C_{ps} = 2.37 \times 10^6\,\mathrm{J\,m^{-3}\,K^{-1}}$ and so $\lambda_w \sim 1.37$. For injection at a rate $Q = Q_o t^\gamma$, three cases arise. If $\gamma < 0$, then the role of the advective heat transport becomes progressively smaller with time, and the rate of change of temperature in the matrix is controlled by conduction, leading to long-time asymptotic similarity solutions for a line source of heat as described by Carslaw & Jaegar (1986). If $\gamma > 0$, then the role of heat conduction becomes progressively smaller with time, and the temperature evolution of the matrix is controlled by advection of heat except across a sharp thermal boundary layer dividing a region near the source with the injection temperature and a warm region with the far-field temperature.

In the intermediate case, $\gamma = 0$, corresponding to constant injection rate, Q, both the advective and conductive heat transport remain important for all time, and the system admits a different class of similarity solutions $T(\eta)$ where $\eta = r/2(\kappa t)^{1/2}$. These solutions illustrate the transition from advection- to diffusion-controlled heat transfer as the flow rate decreases from large values $Q \gg \kappa$ to smaller values $Q \ll \kappa$, and so we focus upon these herein. In these solutions, the interface is located at

$$\eta = \omega = [Q/2\phi\kappa]^{1/2}. \tag{2.4}$$

In similarity coordinates, the diffusion equation becomes

$$-\left(\frac{(1-\lambda_w Q/\kappa)}{\eta} + 2\eta\right)\frac{\mathrm{d}T}{\mathrm{d}\eta} = \frac{\mathrm{d}^2 T}{\mathrm{d}\eta^2} \tag{2.5}$$

with solution

$$T(\eta) = T_o + \Delta T \int_0^\eta \eta^{(\lambda_w\beta-1)}\exp(-\eta^2)\mathrm{d}\eta \tag{2.6}$$

where $\beta = Q/\kappa$ and $\Delta T = (T_2 - T_0)/\int_0^\infty \eta^{(\lambda_w\beta-1)}\exp(-\eta^2)\mathrm{d}\eta$, T_o is the source temperature and T_2 is the far-field temperature. In these solutions there is no net heat flux supplied to the origin for $Q > 0$ since $\eta \mathrm{d}T/\mathrm{d}\eta \to 0$ as $\eta \to 0$. This is a result

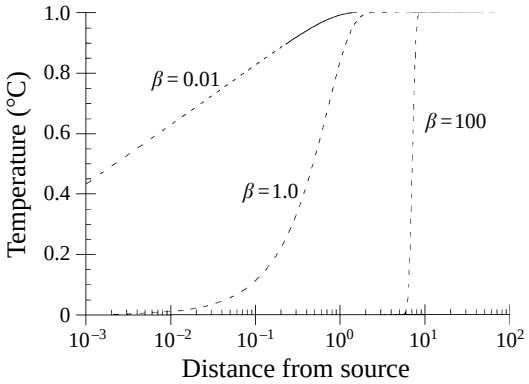

FIGURE 2. Illustration of the dimensionless temperature profile $T(\eta)$ in the newly injected liquid (dashed) and original liquid (solid) for the cases of (i) slow, $\beta = 0.01$; (ii) intermediate, $\beta = 1$ and (iii) fast, $\beta = 100$ injection.

of the advection of fluid away from the source, and contrasts with the temperature field produced by a line source in a solid body, in which there is finite net heat flux transferred to the source (Carslaw & Jaegar 1986). In the present case, the absence of a net heat flux at the origin demands that the temperature at the source $\eta = 0$ equals the initial injection temperature of the liquid.

The temperature at the interface between the newly injected liquid and the original liquid is given by $T_i = T(\omega)$ and has the form

$$T_i = \frac{T_2 \displaystyle\int_0^{\omega} \eta^{\lambda_w \beta - 1} \exp(-\eta^2) \mathrm{d}\eta + T_0 \int_{\omega}^{\infty} \eta^{\lambda_w \beta - 1} \exp(-\eta^2) \mathrm{d}\eta}{\displaystyle\int_0^{\infty} \eta^{\lambda_w \beta - 1} \exp(-\eta^2) \mathrm{d}\eta}. \tag{2.7}$$

In figure 2 we compare the temperature profile for three injection rates, illustrating how the heat transfer differs from the diffusion-limited slow injection case to the advection-limited fast injection case. Figure 3 shows how the interface temperature varies with injection rate. Three thermal regimes may be identified.

Fast injection. For $\beta \lambda_w > 1$ the interface migrates much more rapidly than heat may be conducted from the far field. The liquid is heated to the far-field temperature by cooling the rock near the source and the liquid attains the far-field temperature long before reaching the leading edge of the zone of newly injected liquid. In this advection-limited case, the cold region near the source is divided from the far-field high-temperature region by a sharp internal boundary layer (figure 2, $\beta = 100$).

Intermediate injection. If $\phi < \beta < 1/\lambda_w$, then again the rate of advance of the liquid through the interstices is greater than the rate of heat conduction from the far field. As a result, a large fraction of the newly injected liquid attains the far-field temperature. However, the isotherms are now advected more slowly than the rate of heat conduction and so the internal boundary layer extends back to the source (figure 2, $\beta = 1$). As in the case of very fast injection, the thermal energy used to raise the temperature of the injected liquid originates from the cooling of the rock near the source.

Slow injection. In the case $\beta < \phi$, the liquid front advances much more slowly than the rate of heat diffusion (figure 2, $\beta = 0.01$). Now the newly injected liquid occupies a small inner part of the thermal boundary layer between the source and the

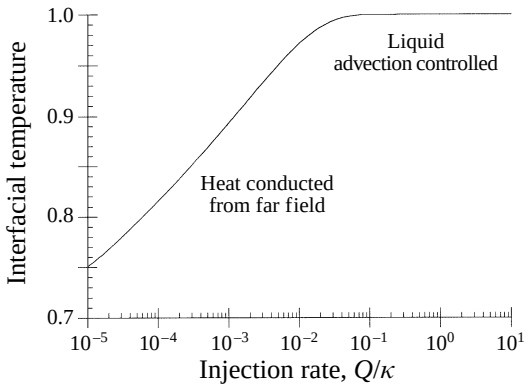

FIGURE 3. Variation of the dimensionless temperature of the interface between the original and the newly injected liquid, $(T_i - T_o)/(T_2 - T_o)$, as a function of the dimensionless injection rate β. For sufficiently high flow rates, the liquid advances ahead of the thermal boundary layer and therefore has a temperature equal to that of the far field.

far field, and some of the original liquid is cooled. The temperature of the interface with the original liquid therefore decreases as the injection rate decreases to values $\beta < \phi$ (figure 3). As the injection rate continues to decrease, the temperature profile approaches the purely diffusive similarity solution for a line source of heat (cf. Carslaw & Jaegar 1986), except in the region $\eta < O(Q/\kappa)$ near the source, in which advection remains important.

We have tested these solutions with a series of laboratory experiments and these are reported in §3. We then extend the model to describe the temperature profile which develops as liquid invades a superheated reservoir. In that case, the interface temperature is constant, but the mass fraction vaporizing changes according to the amount of heat conducted into the interface from the far field.

3. Experimental model of liquid–liquid heat transfer

We have carried out a series of experiments to test the model predictions for injection of liquid into a hot permeable layer saturated with liquid (§2). The apparatus consisted of a cylindrical bed of consolidated permeable sand, of radius 25 cm and 3 cm deep enclosed between two impermeable boundaries of epoxy. The sand bed consisted of 82% 30 mesh sand and 18% Portland cement. Twelve thermocouples were embedded into the sand layer located at 1 cm radial increments from the source, and these were connected to a digital data recorder. Before each experiment, carbon dioxide was injected into the centre of the slab through an injection port in order to displace the air. Cold de-ionized water was then injected in order to displace the CO_2. Any remaining gas dissolved in this water. Insulating material was then placed on the upper and lower surfaces of the epoxy boundaries and the apparatus connected to a water pump and heater.

In each experiment, water was supplied at a constant flow rate. This was varied from experiment to experiment in the range $q \sim 5$–$50\ \mathrm{ml\,min^{-1}}$. For convenience, in the experiments hot water was in fact injected into a cold liquid-filled sand bed, and several experiments were conducted using different flow rates and injection temperatures. After completion of the experiments, two CT scans of the sand layer apparatus were taken, one with the core fully dry and one with the core fully saturated

with liquid. Using these measurements, the porosity was estimated to be 35 $\pm$3%. Using this estimate together with the known properties of the sand, $C_{ps} = 950 \pm 50\,\mathrm{J\,K^{-1}\,kg^{-1}}$, $\rho_s C_{ps}\kappa_s = 5.2\,\mathrm{W\,m^{-1}\,K^{-1}}$ and $\rho_s = 2500\,\mathrm{kg\,m^{-3}}$, and the liquid water $C_{pl} = 4216\,\mathrm{J\,K^{-1}\,kg^{-1}}$, $\rho_l C_{pl}\kappa_l = 0.681\,\mathrm{W\,m^{-1}\,K^{-1}}$ and $\rho_l = 961\,\mathrm{kg\,m^{-3}}$, the effective thermal diffusivity of the porous medium was calculated to be $1.23 \pm 0.1 \times 10^{-6}\mathrm{m^2\,s^{-1}}$ using the relationship (Batchelor 1974)

$$\kappa = \frac{\phi\kappa_l C_{pl}\rho_l + (1-\phi)\kappa_s C_{ps}\rho_s}{\phi C_{pl}\rho_l + (1-\phi)C_{ps}\rho_s}. \tag{3.1}$$

During each experiment, temperature measurements were made at several times. In figure 4, we compare these temperature profiles with the theoretical prediction for $\beta = 0.67$ and $\beta = 3.4$. In both cases, $\lambda_w \approx 1.37$. The radial locations of these measurements have been non-dimensionalised, $\eta = r/(\kappa t)^{1/2}$, and the temperature profiles are shown as a function of η. For both the fast injection case $\beta = 3.4$ and the slower injection case $\beta = 0.67$, the experimental results collapse very accurately onto the theoretical temperature profiles. These experimental results support the thermal picture of fast injection described in Part 1, in which the liquid was assumed to attain the vaporization temperature some distance behind the interface. We now build on these results to analyse the vaporization associated with slow liquid injection into a superheated reservoir.

4. Liquid injection into a vapour-saturated superheated reservoir

If the reservoir is superheated and vapour saturated, then a fraction f of the liquid may vaporize as the liquid invades the reservoir. In Part 1, we described the case of high flow rates for which the dynamic vapour pressure, required to drive new vapour ahead of the boiling front, becomes important (see the Appendix) and conduction of heat from the far-field is negligible. We found that as the liquid supply rate increases, the vapour pressure at the interface also increases. This allows the saturation temperature at the interface to approach the far-field reservoir temperature, thereby reducing the superheat available for vaporization and decreasing the mass fraction of liquid which vaporizes.

In the present work, we consider smaller flow rates, $Q \leqslant 10^{-1}$-$10^{-3}\ \mathrm{m^2\,s^{-1}}$, for which the dynamic vapour pressure is small (see the Appendix). We therefore approximate the vapour pressure as being constant and equal to that of the far field. In this case, the vapour migrates ahead of the boiling front with Darcy speed $fQ\rho_l/r\rho_v$, where the flux of vapour produced at the boiling front is fQ and ρ_v is the vapour density; for convenience henceforth we refer to f as the mass fraction which vaporizes. The temperature in the vapour is governed by the advection–diffusion equation

$$\frac{\partial T}{\partial t} + \frac{f\lambda_v Q}{r}\frac{\partial T}{\partial r} = \frac{\kappa_2}{r}\frac{\partial}{\partial r}\left(r\frac{\partial T}{\partial r}\right) \tag{4.1}$$

where κ_2 is the average diffusivity of the vapour and solid matrix (cf. (2.2)) and $\lambda_v = \rho_v C_{pv}/(\phi\rho_v C_{pv} + (1-\phi)\rho_s C_{ps})$ is the dimensionless specific heat of the vapour. $\lambda_v \approx 6.4 \times 10^{-4}$ at atmospheric pressure in porous sandstone of porosity 0.19, using the properties $C_{pv} = 2028\,\mathrm{J\,kg^{-1}\,K^{-1}}$, $\rho_v \sim 0.6\,\mathrm{kg\,m^{-3}}$ and $\rho_v C_{pv}\kappa_v = 0.025\,\mathrm{W\,m^{-1}\,K^{-1}}$. Typically, for $\phi \ll 1$, $|\kappa_2 - \kappa| \ll \kappa$, and so for simplicity in the following analysis we assume that $\kappa_2 \sim \kappa$, although the model may be readily extended to account for this difference. The temperature in the liquid is again governed by equation (2.1). At the

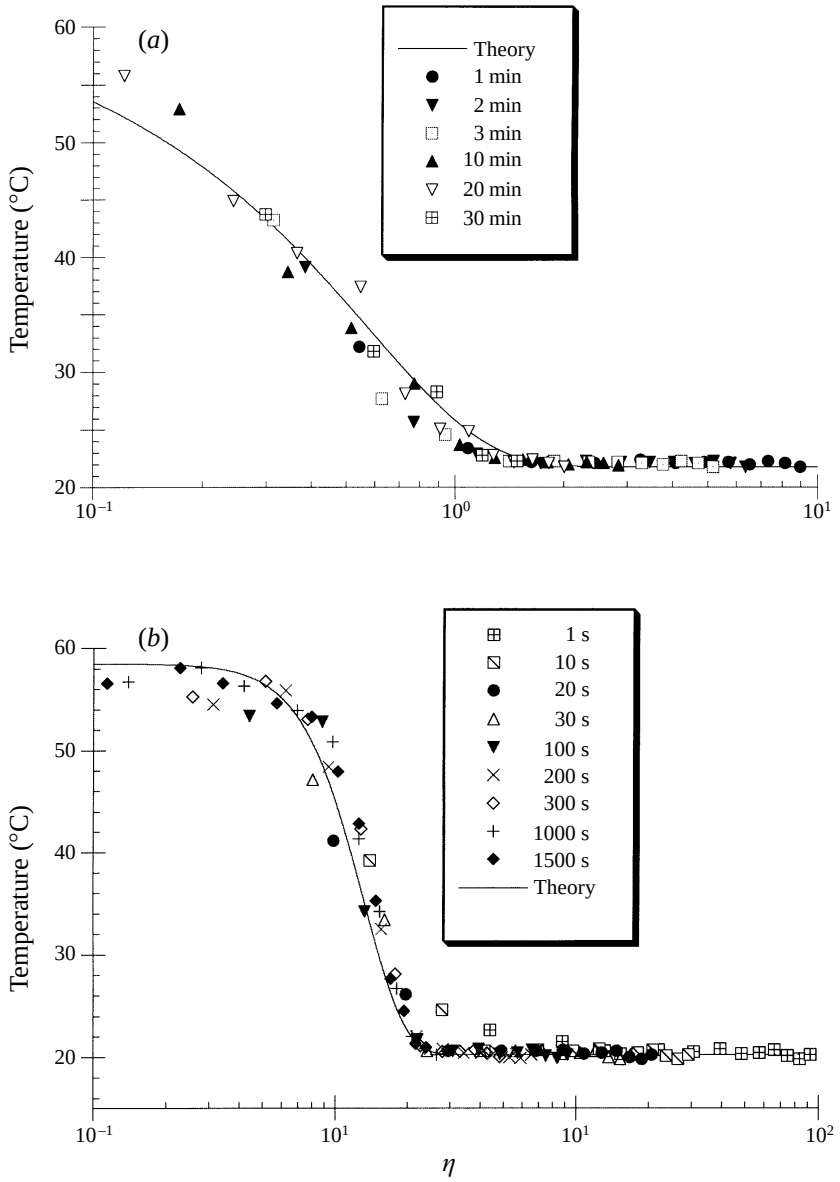

FIGURE 4. Comparison of the model predictions with experimental measurements of temperature as a function of distance from the source. Distances are shown in dimensionless form $\eta = r/(2\kappa t)^{1/2}$. Results are shown for two experiments in which hot liquid is injected into a cold water saturated layer. (*a*) $\beta = 0.67$, T(input)=63°C and T(initial)=20.2°C and (*b*) $\beta = 3.42$, T(input)=59°C and T(initial)=21°C. Symbols show the temperature at different times during the experiment. The solid lines correspond to the theoretical prediction.

interface between the liquid and vapour, the conservation of heat takes the form

$$\left[\frac{\partial T}{\partial r}\right]_{-}^{+} = \frac{fQ\rho_l L}{\kappa\rho C_p r} \tag{4.2}$$

where L is the latent heat of vaporization and $\kappa\rho C_p = \phi\kappa_l\rho_l C_{pl} + (1-\phi)\kappa_s\rho_s C_{ps}$ is the mass averaged thermal conductivity of the solid matrix and fluid, defined in terms of

the density and specific heat of the constituents (cf. (3.1)). The temperature is given by the Clausius–Clapeyron relation $T = T_s(P)$ while, as in §2, the temperature at the source, $\eta = 0$, equals the initial temperature T_o.

For a constant source of liquid, Q, the system admits similarity solutions in which f is a constant and, as in §2, in these solutions, both the advection and conduction of heat are important. The temperature distribution is given in terms of the similarity variable $\eta = r/2(\kappa t)^{1/2}$ by

$$T(\eta) = T_s + A\int_{\omega}^{\eta} \eta^{[\lambda_v f Q/\kappa - 1]} \exp(-\eta^2)\mathrm{d}\eta \quad \text{for} \quad \eta > \omega \tag{4.3}$$

and

$$T(\eta) = T_s + B\int_{\omega}^{\eta} \eta^{[\lambda_w Q/\kappa - 1]} \exp(-\eta^2)\mathrm{d}\eta \quad for \quad \eta < \omega \tag{4.4}$$

where the boiling interface is located at

$$\eta = \omega = [Q(1-f)/2\phi\kappa]^{1/2}. \tag{4.5}$$

The constants A and B and the mass fraction of the injected liquid which vaporizes, f, are given in terms of the reservoir superheat, $T_2 - T_s$, the initial liquid undercooling, $T_o - T_s$, and the injection rate Q. The conservation of heat at the interface, $\eta = \omega$, has the form

$$B\omega^{[Q\lambda_w/\kappa]} \exp(-\omega^2) - A\omega^{[fQ\lambda_v/\kappa]} \exp(-\omega^2) = -\frac{LfQ}{\kappa C_p}. \tag{4.6}$$

The continuity of temperature at the source, $\eta = 0$, requires

$$T_o = T_s + B\int_{\omega}^{0} \eta^{[\lambda_w Q/\kappa - 1]} \exp(-\eta^2)\mathrm{d}\eta \tag{4.7}$$

and in the far field, $\eta \to \infty$,

$$T_2 = T_s + A\int_{\omega}^{\infty} \eta^{[\lambda_v f Q/\kappa - 1]} \exp(-\eta^2)\mathrm{d}\eta. \tag{4.8}$$

We have solved equations (4.6)–(4.8) to determine how the mass fraction which vaporizes, f, varies with (i) the ratio of the injection rate to the thermal diffusivity, $\beta = Q/\kappa$; (ii) the ratio of the initial liquid undercooling to the reservoir superheat, $u = (T_s - T_o)/(T_2 - T_s)$; and (iii) the ratio of the latent heat of vaporization to the initial reservoir superheat, $S = L/C_p(T_2 - T_s)$. The results are shown in figure 5, where it is seen that the mass fraction vaporizing smoothly decreases from a value close to unity to a smaller, near-constant value f_f say, as the flow rate increases to values $\beta > O(1)$. The high-flow-rate value f_f decreases as the latent heat of vaporization increases, but is independent of the initial undercooling of the liquid. However, as the undercooling increases, the critical flow rate at which the mass fraction vaporizing first begins to decrease is smaller. These controls on the mass fraction which vaporizes may be understood by reference to detailed thermal profiles corresponding to different flow rates. In figure 6 we present temperature profiles in the liquid and vapour for three different injection rates, focusing on the slow injection rate regime in figure 6(*a*) ($\beta = 0.006$) and the fast regime in figure 6(*b*) ($\beta = 7.4$).

Fast flow: $\lambda_w\beta > 1$. For high injection rates, the Darcy velocity of the liquid exceeds the rate of thermal diffusion and so heat cannot be conducted back to the source. Near the source, the liquid temperature remains close to the injection temperature

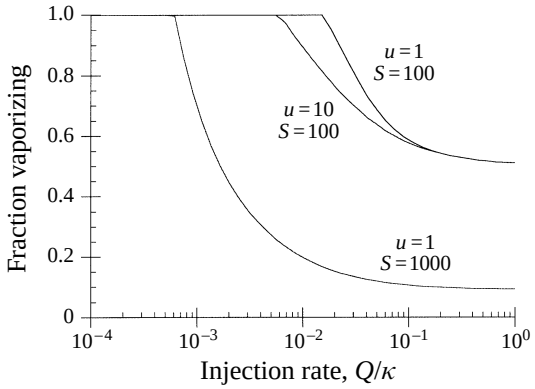

FIGURE 5. Variation of the mass fraction of liquid which vaporizes, f, as a function of the dimensionless injection rate, β. Curves are shown for two values of the dimensionless undercooling, $u = (T_s - T_o)/(T_2 - T_s)$, $u = 1, 10$ and of the latent heat of vaporization $S = L/C_p(T_2 - T_s)$, $S = 100, 1000$ of the reservoir.

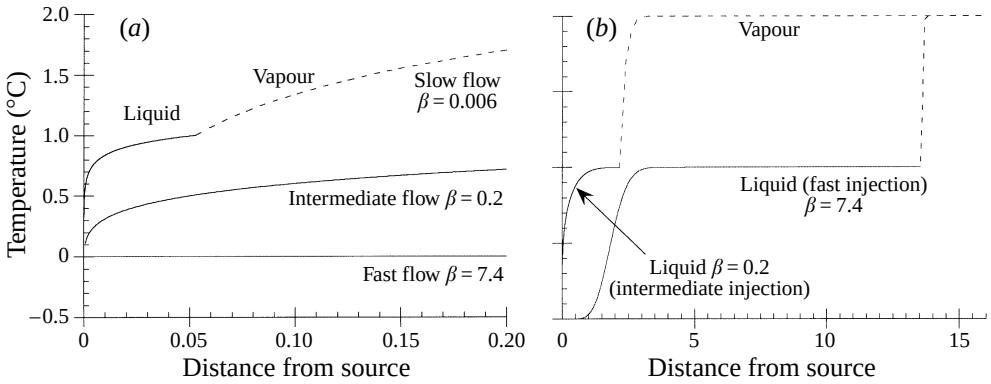

FIGURE 6. Illustration of the temperature profile, $T(\eta)$, in the liquid and vapour for the cases of (i) slow, $\beta = 0.006$; (ii) intermediate, $\beta = 0.2$ and (iii) fast, $\beta = 7.4$ injection. The liquid is shown by the solid lines and vapour by the dashed lines. (*a*) The structure near the source, (*b*) the structure further from the source. In this plot, the temperature of the liquid is 0, the boiling temperature is 1 and the far-field vapour temperature is 2.

T_o (figure 6*a*,*b*, $\beta = 7.4$). Once the liquid has invaded a distance $\eta \sim O((\lambda_w\beta - 1)^{1/2})$, a narrow thermal boundary layer develops and the liquid is rapidly heated to the vaporization temperature. The liquid then migrates through a nearly isothermal zone to the boiling interface. The boiling interface advances sufficiently rapidly that there is negligible heat conducted into the liquid from the far-field. Asymptotically, the mass fraction vaporizing then depends only on the reservoir superheat

$$f \sim \frac{1}{1 + L\phi/C_p(T_2 - T_s)} = \frac{1}{1 + S\phi}. \tag{4.9}$$

This limit corresponds to the slow injection regime studied in Part 1 in which vapour pressure effects were not important. The mass fraction vaporizing is independent of the initial temperature of the liquid but increases with the reservoir superheat since more energy is released by the rock as it is cooled by the invading liquid.

Intermediate flow: $\beta\lambda_w < 1 < \omega$. In this case, the Darcy velocity of the liquid is

comparable to the rate of thermal diffusion, and so the internal thermal boundary layer now extends back to the origin (figure 6*a*, $\beta = 0.2$). However, since the boiling front migrates more rapidly than the rate of thermal diffusion, the liquid is heated up to the interfacial temperature long before reaching the interface. Therefore, a large isothermal liquid region again develops behind the boiling front, and the mass fraction vaporizing has the asymptotic form (4.9). The difference between this case and the fast injection case may be of interest for interpreting field data, since near to the well very different thermal profiles develop.

Slow flow: $\omega < 1$. If the interstitial speed of the liquid is small compared to that of thermal diffusion, then the thermal boundary layer extends from the cold source through the whole liquid region and beyond the boiling front into the vapour (figure 6*a*, $\beta = 0.006$). As a result, there is a significant heat flux conducted from the region ahead of the interface into the liquid zone. This cooling of the vapour zone increases the rate of vaporization and in the limit of very small injection rates, $\beta \ll 1$, $f \to 1$. As for the liquid–liquid case (§2), there is no net heat flux supplied to the origin, $\eta = 0$, so that a small region of liquid spreads from the origin. However, conduction of heat from the superheated reservoir far ahead of the boiling front provides so much heat that most of the liquid vaporizes.

Using the same experimental method as described in §3, we conducted a series of further laboratory experiments in which liquid water was injected into a porous cylindrical bed of sandstone, of thickness 2.4 cm and radius 25 cm, and porosity $\phi = 0.19 \pm 0.1$. The bed was preheated to temperatures in the range 105–120°C. Using the thermal properties of the sandstone and water (cf. §3) $\kappa = 1.6 \pm 0.1 \times 10^{-6} \mathrm{m^2\,s^{-1}}$ (cf. (3.1)), while $\lambda_w \sim 1.5$ (cf. (2.3)). In figure 7, we present data from a typical experiment in which the flow rate was 10 $\mathrm{ml\,min^{-1}}$, corresponding to $\beta = 0.7$ with the source temperature 73°C and initial sandstone temperature of 109°C. The temperature was measured by thermocouples located at 12 different radii in the bed, and the temperature of each thermocouple was recorded at 5 s intervals. In the figure, the temperature record of each thermocouple is plotted as a function of the similarity variable $\eta = r/(\kappa t)^{1/2}$. The measurements are compared with the corresponding similarity solution for $\beta = 0.7$ (solid line), using the value $L = 2088\,\mathrm{J\,kg^{-1}}$ for the latent heat of vapour at 100°C (Haywood 1972). Again, there is very good agreement between the model similarity solution and the experimental data.

5. Extension to model fractured rock

5.1. *Permeable regions*

The model presented in §§2 and 4 applies to an isolated permeable layer of cylindrical geometry in which the flow and heat transfer is purely radial. The solutions may be applied to examine the flow in a relatively deep porous sedimentary layer in which the effects of cross-flow heat transfer are small. As long as the along-flow conduction length, $(\kappa t)^{1/2}$, is smaller than the width of the layer, D say, then cross-flow heat transfer is small, and the solutions of §§2 and 4 apply. For example, the Cerro Prieto geothermal field in northern Mexico includes several deep layers of sediment of nearly 100 m vertical extent (Truesdell *et al.* 1995). Therefore, the model is appropriate for times much smaller than $\tau \sim 10^{10}\mathrm{s} \sim 100$ years.

Typical liquid injection rates in geothermal reservoirs lie in the range $10^{-4} - 10^{-2}$ $\mathrm{m^2\,s^{-1}}$. For such rates, the liquid spreads more rapidly than the rate of thermal diffusion (§2) and for injection into a water-saturated non-superheated reservoir, the

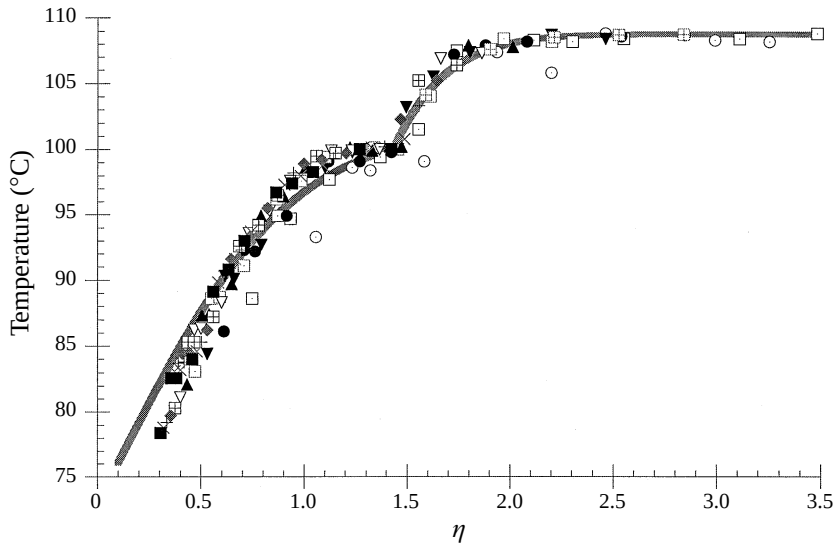

FIGURE 7. Comparison of the similarity theory with a laboratory experiment in which water, with initial temperature 73°C, was injected into a superheated cylindrical sandstone bed of initial temperature 109°C. In the experiment, the injection rate was $10\,\mathrm{ml\,min^{-1}}$, corresponding to $\beta = 0.7$. Temperature measurements for twelve different thermocouples which were located at various radii from the centre of the sandstone bed are shown at 12 times during the course of the experiment. The temperature of each thermocouple is shown as a function of the similarity variable $\eta = r/(\kappa t)^{1/2}$. These are compared with the theoretical similarity solution predicted in §4 (solid line).

temperature profile follows the fast regime of §2. For injection at rates $10^{-4} - 10^{-2}$ $\mathrm{m^2\,s^{-1}}$ into a superheated zone, vapour pressure effects are small (see the Appendix) and the fast regime of §4 applies. Equation (4.9) then suggests that for typical reservoir superheats of the order of a few degrees, the Stefan number of vaporization, S, takes values of order 10–100 (cf. Part 1), and the model predicts that the mass fraction of liquid which vaporizes lies in the range 0.2–0.6.

5.2. *Multiply fractured rock*

The model is also of some use for examining liquid flow into a multiply fractured rock. The similarity solutions describe the liquid migration and vaporization within permeable fractures at very small and at long times. For very small times, the cross-fracture heat transfer is small, and the similarity solutions of §§2 and 4 apply for the individual fractures. For permeable fractures of width 0.1 mm–1 cm, and typical thermal diffusivities of order $10^{-7}\mathrm{m^2\,s^{-1}}$, this regime will thus apply for times $\tau \ll 0.1$–1000 s.

In contrast, over very long times, $t \gg d^2/\kappa$, where d is the mean interfracture distance, heat transfer between the fractures and the neighbouring rock will become relatively rapid, and the fracture–host rock system will thermally equilibrate in the cross-fracture direction. For fracture spacings of 0.1–1 m, the system requires of order 0.1–1 years to equilibrate. Assuming that the fractures are uniformly distributed throughout the rock, so as to produce an effectively uniform permeability on a scale larger than the fractures (cf. Dullien 1992; Fitzgerald & Woods 1995), then the flow will on average be directed away from the source. The solutions of §§2 and 4 again apply, but now in terms of the average porosity of the fractures and host rock. In this long-time regime, heat is supplied to the boiling front from the host rock, thereby

increasing the mass fraction of liquid which boils. Indeed, for fractures with internal porosity of order ϕ_f, embedded in a host rock with an effective macro-porosity ϕ_m, then, according to the fast flow regime (§4, (4.9)), the fraction which vaporizes increases by a factor $(1+S\phi_f)/(1+S\phi_m)$, and the front speed decreases by the same factor.

5.3. *Anisotropic permeability structure*

In many cases, there is a preferred direction along which the permeability exceeds that in the other directions, possibly owing to alignment of small fractures or of grains in layered sediment deposits. For such an anisotropic medium, we can apply the results of §4 to model the two-dimensional flow of the vaporizing front from a well in the relatively rapid liquid flow regime, $Q \sim 10^{-2} - 10^{-4}$ m^2 s^{-1}. This regime is appropriate for injection in many geothermal systems (§5.1) and applies if liquid invades the reservoir more rapidly than heat may be conducted from the far-field, and also if there is negligible dynamic pressure associated with the migration of the vapour ahead of the interface (see the Appendix). In this case, a sharp thermal boundary layer develops at the boiling front, across which the vapour is heated from the boiling point to the temperature of the far field. A second thermal boundary layer develops within the liquid zone, across which the liquid is heated from the injection temperature to the boiling point, although this boundary layer is some distance behind the interface.

If we denote the permeability as k_x in the preferred flow direction, x, and k_y normal to this direction, then for the fast flow regime liquid injected at a constant rate Q will spread elliptically, so that after time t it fills the region

$$x^2 k_y + y^2 k_x \leqslant fQt(k_x k_y)^{1/2}/\phi. \tag{5.1}$$

Here f is the constant mass fraction of liquid which vaporizes and is given by (4.9). The result applies as long as the rate of advance of the liquid in the less-permeable y-direction far exceeds the rate of diffusion of heat

$$fQ(k_y/k_x)^{1/2} \gg \phi\kappa \tag{5.2}$$

so that f is independent of direction. For typical liquid flow rates Q, per unit length along the injection well, in the range $0.01 - 0.0001$ m^2 s^{-1}, condition (5.2) is satisfied for permeability ratios $k_y/k_x > 10^{-8} - 10^{-12}$. We also require the vapour pressure scale (see the Appendix) to be greater than the distance travelled by the advancing layer of newly formed vapour, so that there is no pressure build up in the advancing layer of vapour. For a layer in which the dominant permeability k_x has value $10^{-12} - 10^{-14}$ m^2, the dynamic vapour pressure is small when (cf. (A5)) $fQ \ll (0.01 - 1.0)(k_y/k_x)^{1/2}$. Comparing this with typical geothermal injection rates $0.0001 - 0.01$ m^2 s^{-1}, we deduce that the solutions (5.1) are valid when $k_y/k_x > 10^{-4}$; for smaller permeability ratios, the dynamic vapour pressure becomes significant, thereby reducing the mass fraction which vaporizes. Since the permeabilities of fractured rock are typically of order $10^{-12} - 10^{-16}$, the solution (5.1) thus provides a powerful approximation for a wide range of realistic injection conditions in geothermal systems.

6. Summary

In this contribution we have derived similarity solutions to describe the evolution of the temperature as cold liquid is injected into a porous layer initially saturated with hot liquid. The solutions identify that for slow injection heat diffusion from the

far field is dominant and so some of the original fluid in the porous layer is cooled in order to heat up the newly injected liquid. For faster injection, the leading edge of the newly injected liquid advances so rapidly that there is negligible conduction of heat from the far field and little cooling of the original liquid. Instead, a region of the host rock around the source is cooled, and this provides the thermal energy to heat up the newly injected liquid to the original temperature of the permeable layer. For sufficiently large flow rates, the isotherm advection speed through the porous layer exceeds the rate of heat conduction. As a result, the inner region, which is cooled to the injection temperature of the liquid, is separated from the outer region, whose temperature equals that of the far field, by a sharp internal boundary layer. We have confirmed these theoretical predictions with a series of laboratory experiments in which liquid of one temperature was injected into a porous layer saturated with liquid of a second temperature.

We then extended the analysis to consider the slow injection of cold liquid into a superheated permeable layer initially saturated with vapour, thereby complementing Part 1 in which we considered fast injection. We have found that two main vaporization regimes develop depending on the liquid injection rate in comparison with the rate of thermal diffusion. For small injection rates, heat may be conducted from the far field into an advancing layer of liquid, and so the mass fraction of the liquid which boils increases towards unity. For higher flow rates, this conductive heat transfer becomes ineffective. Instead, as the liquid invades the hot permeable rock, the cooling of the rock near the source heats the liquid to the vaporization temperature, and a large region of nearly isothermal liquid, with the vaporization temperature, develops behind the boiling front. The liquid then boils as it invades the hot rock, with the mass fraction which vaporizes being controlled by the release of the superheat of the rock. Again we successfully tested the predictions of the model with a laboratory experiment in which liquid water was injected into a superheated bed of sandstone.

Appendix

The dynamics of the vapour migrating ahead of the interface may be described using Darcy's Law, appropriate for the low-Reynolds-number flow through the pore spaces (Fitzgerald & Woods 1995)

$$\mu u = -k\nabla P \tag{A 1}$$

where k is the permeability and μ the dynamic viscosity of the vapour, which remains approximately constant over the typical range of pressures in a geothermal reservoir (Pruess *et al.* 1987; Haywood 1972). If we couple this with an equation of state for the vapour

$$P = \rho_v RT \tag{A 2}$$

and the equation for mass conservation

$$\phi\frac{\partial \rho}{\partial t} + \nabla \cdot \boldsymbol{u}\rho_v = 0 \tag{A 3}$$

we obtain the dynamic equation for the vapour

$$\frac{\partial}{\partial t}\left(\frac{P}{T}\right) = \frac{k}{\phi\mu}\nabla \cdot \left(\frac{P}{T}\nabla P\right). \tag{A 4}$$

This equation identifies that the vapour pressure evolves over a typical length scale $L_p \sim (kPt/\phi\mu)^{1/2}$. The ratio of the pressure-evolution length scale, L_p, to

the temperature-evolution length scale, $L_t \sim (\kappa t)^{1/2}$, given by $(kP/\phi\mu\kappa)^{1/2}$ is typically of order $10^3 - 10^4$ for systems of permeability $10^{-12} - 10^{-14}$ m^2 and porosity 10^{-2} (§2.1). We deduce that the pressure remains nearly constant across any thermal boundary layers associated with the migration and vaporization of liquid in a porous layer (Part 1).

Furthermore, the dynamic vapour pressure associated with the production of new vapour at the interface only becomes a significant fraction of the background reservoir pressure if the advancing region of newly formed vapour, $(fQ\rho_v t/\rho_l)^{1/2}$, exceeds the pressure length scale L_p (cf. Fitzgerald & Woods 1995). This requires

$$fQ > \frac{kP\rho_l}{\phi\mu\rho_v}. \tag{A 5}$$

For typical permeabilities of the order 10^{-12}–10^{-14} m^2, this requires injection rates Q greater than 1.0–0.01 m^2 s^{-1}. Therefore, the thermal models in the present paper are only valid for dimensionless injection rates $\beta = Q/\kappa < 10^4 - 10^6$ (§§2–4). For higher injection rates, the effects of vapour pressure would become important and the effects described in Part 1 dominate.

REFERENCES

Barker, B. J., Koenig, B. A. & Stark, M. A. 1995 Water injection management for resource maximization: observations from 25 years at The Geysers, California. *Proc. World Geothermal Congr.* **3**, 1959–1964.

Batchelor, G. K. 1974 Transport properties of two-phase materials with random structure. *Ann. Rev. Fluid Mech.* **6**, 227–255.

Carslaw, H. S. & Jaeger, J. C. 1986 *Conduction of Heat in Solids.* Oxford University Press.

Dullien, F. A. L. 1992 *Porous Media – Fluid Transport and Pore Structure.* Academic.

Elder, J. 1981 *Geothermal Systems.* Academic.

Enedy, S. L., Smith, J. L., Yarter, R. E., Jones, S. M. & Cavote, P. E. 1993 Impact of injection on reservoir performance in the NCPA steam field at The Geysers. *Proc. Stanford Geothermal Workshop* **18**, 125–134.

Fitzgerald, S. D. & Woods, A. W. 1995 On vapour flow in a hot porous layer. *J. Fluid Mech.* **293**, 1–23.

Grant, M. A., Donaldson, I. G. & Bixley, P. F. 1982 *Geothermal Reservoir Engineering.* Academic.

Haywood, R. W. 1972 *Thermodynamic Tables in SI (Metric) Units.* Cambridge University Press.

Pruess, K., Calore, C., Celati, R. & Wu, Y. S. 1987 An analytical solution for heat transfer at a boiling front moving through a porous medium. *Intl J. Heat Mass Transfer* **30**, 2595–2602.

Truesdell, A. H., Lippmann, M. J., Quijano, J. L. & D'Amore, F. 1995 Chemical and physical indicators of reservoir processes in exploited high-temperature liquid-dominated geothermal fields. *Proc. World Geothermal Congr.* **3**, 1933–1938.

Woods, A. W. & Fitzgerald, S. D. 1993 The vaporization of a liquid front moving through a hot porous rock. *J. Fluid Mech.* **251**, 563–579 (referred to herein as Part 1).